Articles

Structural and Dynamic Changes in Human Annexin VI Induced by a Phosphorylation-Mimicking Mutation, T356D[†,‡]

Caroline Freye-Minks,[*,§] Robert H. Kretsinger,[||] and Carl E. Creutz[§]

Departments of Pharmacology and Biology, University of Virginia, Charlottesville, Virginia 22908

Received August 27, 2002; Revised Manuscript Received November 15, 2002

ABSTRACT: Phosphorylation of some members of the annexin family of proteins may play a significant role in controlling their calcium-dependent interactions with membranes. Recent electron microscopic studies of annexin VI revealed that the protein's two core domains exhibit a great degree of flexibility and are able to undergo a relative conformational change that could potentially initiate contacts between membranes [Avila-Sakar, A. J., et al. (2000) *J. Struct. Biol. 130*, 54−62]. To assess the possibility of a regulatory role of phosphorylation in this behavior, the crystal structure of a phosphorylation-mimicking mutant (T356D in the flexible connector region of human annexin VI) was determined to 2.65 Å resolution. When the mutant is compared to the wild-type annexin VI, subtle differences are seen at the site of the mutation, while larger changes are evident in one of the calcium-binding loops and in the presence of five calcium ions. Furthermore, biochemical studies provide evidence for additional conformational differences between the T356D and wild-type solution structures. Fluorescence emission and acrylamide quenching suggest a higher level of solvent exposure of Trp-343 in the connector region of T356D in the presence of calcium. Comparisons of retardation coefficients in native gel electrophoresis reveal that T356D has a more extended shape, while proteolytic studies show a greater accessibility of a trypsin cleavage site inside the linker region, indicating a conformation more open than the wild-type form. These data provide insights into a possible regulatory mechanism leading to a higher degree of flexibility and possibly a higher calcium binding affinity of annexin VI upon phosphorylation.

The annexins are a family of soluble proteins capable of binding phospholipids in a calcium-dependent manner (*1*). Some members of the family are believed to participate in a variety of membrane−membrane interactions due to their ability to aggregate phospholipid vesicles and biological membranes (*2*), although their physiological functions have not been determined with certainty.

Serine, threonine, and tyrosine phosphorylation of annexins occurs preferentially in the unique N-terminal domains of the proteins. Although it is known that these phosphorylations take place in vivo, their physiological significance remains the subject of investigation. However, in vitro experiments reveal significant impacts of phosphorylation on the membrane binding and lipid aggregation properties of various annexins (see ref *3* for an overview).

This study focuses on the impact of phosphorylation on the structural and functional properties of annexin VI. Annexin VI is the only member of the annexin family that contains eight "endonexin fold" repeats instead of four and has approximately twice the molecular mass of other annexins (70 kDa). This organization presumably arose from gene duplication during evolution (*4*). The eight repeats are organized into two core domains of four repeats, each with a disklike shape. The two disks or lobes are connected through a flexible connector. The crystal structure of annexin VI reveals a perpendicular orientation of its two lobes (*5*, *6*) that can be observed in both the calcium-bound and calcium-free forms. Once membrane binding takes place, a conformational change seems to take place, as indicated by electron micrographs of two-dimensional crystals of annexin VI on lipid monolayers (*5*, *6*), allowing the two planes of the cores to face a single membrane in a "parallel" manner. However, recent three-dimensional images of membrane-bound annexin VI reveal that one of the cores may twist 180° about the flexible linker (*7*). The resulting "antiparallel" orientation is surprising, as the convex face of one of the lobes, with its high affinity for phospholipids, would thus face away from the membrane. Nevertheless, in this position, the protein might be able to bind two closely apposed membranes simultaneously.

It has been reported that annexin VI becomes phosphorylated in murine Swiss 3T3 fibroblasts in a growth-dependent manner on serine and threonine (*8*). Although these sites of phosphorylation have not been mapped, it seems likely they represent the canonical phosphorylation

[†] Supported by NIH Research Grants GM53266 and GM59891.

[‡] Coordinates have been deposited in the Protein Data Bank (entry 1M9I).

* To whom correspondence should be addressed. Phone: (434) 982-1617. Fax: (434) 982-3878. E-mail: cf9c@virginia.edu.

[§] Department of Pharmacology.

[||] Department of Biology.

10.1021/bi026742h CCC: $25.00
Published on Web 12/28/2002

site at the N-terminus of annexin VI (Ser-13) and the homologous site in the linker between the two core lobes (Thr-356). Comparison of phosphorylation sites in annexin IV and the conformation of similar sites in annexin VI in the extended coils preceding domains I and V (Ser-13 and Thr-356) reveal a remarkable structural similarity to each other. Ser-13 and Thr-356 are buried in pockets of repeats I and V, and are surrounded by a similar hydrogen bond network with both residues inaccessible to the solvent (*7*). For phosphorylation to occur, Thr-356 must emerge from the pocket and possibly propagate a structural change through the polypeptide chain to the region of the intercore linker. This mechanism could regulate the flexibility of annexin VI to bind either one membrane with both cores in a "parallel" orientation or two membranes in the antiparallel orientation in the cell and in the latter case initiate contacts between two independent membranes.

To probe the effects of phosphorylation of Thr-356, we determined the crystal structure of a phosphorylation-mimicking mutant (T356D)[1] to assess any conformational changes in the three-dimensional structure. In addition, we performed a detailed biochemical characterization of T356D to study differences in the dynamic properties of the phosphorylation-mimicking mutant in terms of calcium binding, flexibility, stability in solution, and membrane interactions.

MATERIALS AND METHODS

Construction of Yeast Expression Vectors for Wild-Type and T356D Mutant Human Annexin VI. An expression plasmid encoding wild-type human annexin VI (without the splice insert in the seventh repeat) was a gift from S. Moss at University College London (London, U.K.). The coding sequence was amplified by PCR using primers that introduced *Sal*I and *Hin*dIII restriction sites adjacent to the initiation codon and termination codon, respectively (*Sal*I primer, 5′-GGC GTC GAC ATG GCC AAA CCA GCA CAGGGT G-3′; *Hin*dIII primer A, 5′-CGC AAG CTT CTA GTC CTC ACC ACC ACA GAG-3′), and the product was ligated into the yeast expression vector YepDB60, which drives expression under the control of the *GAL10* promoter (*9*).

To introduce the T356D mutation, the portions of the cDNA encoding the two lobes of annexin VI were amplified by PCR independently, introducing a new *Hin*dIII site in the linker region [causing silent changes in the codons for Ala-371 (GCG to GCT) and Leu-372 (CTG to TTG)] and changing the codon for Thr-356 (ACT) to GAT (Asp) as follows. DNA encoding the first lobe and the connecting region were amplified using the *Sal*I primer described above with a new *Hin*dIII mutagenizing primer (5′-CGC AAA GCT TTG GCA TCT GCG TCA GGG TTG AAG TCA TTG GCT GGG CGC ACA TCT CCC TTC AGC-3′). The product was ligated into YepDB60 cut with *Sal*I and *Hin*dIII; DNA encoding the second lobe was amplified using the *Hin*dIII primer A described above and a new *Hin*dIII primer B (5′-GCC AAA GCT TTG CGG AAA GCC ATG AAG GGA CTC G). The product was ligated into YepDB60 encoding the mutagenized first lobe and connecting linker cut with *Hin*dIII, and the correct orientation was determined by restriction mapping. The mutation was verified by sequencing of the expression plasmid and of the protein product after cleavage in the linker region by trypsin.

Expression and Isolation of Recombinant Annexin Proteins. Saccharomyces cerevisiae strain NY606 (P. Novick, Yale University, New Haven, CT) or protease deficient strain DB334^{pep4-} (D. Burke, University of Virginia) harboring the annexin VI expression vectors described above was grown in a synthetic galactose-containing minimal medium to a cell density of 8×10^7 cells/mL as described previously (*10*). At this density, the cells were harvested by centrifugation and pellets were resuspended in 50 mM Hepes (pH 7.4), 5 mM EGTA, and 150 mM NaCl and stored at −80 °C. Ten grams of yeast pellet was processed by milling with glass beads in a Biospec Products (Bartelsville, OK) Bead-beater for 10 cycles of 90 s each with a resting time of 60 s on ice between cycles. The resulting crude cell extract was further purified by reversible calcium-dependent binding to artificial lipid vesicles as described previously (*10*). Briefly, after a low-speed and a high-speed centrifugation step at 10000*g* and 100000*g*, respectively, the soluble fraction was combined with artificial liposomes [from 300 mg of brain lipid extract (Sigma product B1502, containing 50% phosphatidylserine), resuspended in 10 mL of 50 mM Hepes (pH 7.4) and 150 mM NaCl, sonicated for 1 min, and washed in the same buffer] and 8 mM Ca^{2+}. After the annexin was allowed to bind to the lipids for 5 min on ice, the liposomes were collected at 20000*g* for 15 min and washed with 50 mM Hepes (pH 7.4) and 2 mM $CaCl_2$ and then with 50 mM Hepes (pH 7.4), 2 mM $CaCl_2$, and 150 mM NaCl. The bound annexin was released from the lipid fraction by resuspension in 20 mM Hepes (pH 7.4) and 10 mM EGTA at least twice. The protein fractions were applied to a Poros Q (PerSeptive Biosystems) column and eluted with a linear 0 to 1 M KCl gradient. After ion exchange, the buffer was changed to 20 mM Tris-HCl (pH 7.4) by ultrafiltration, and the homogeneity of the isolated protein was judged by SDS−PAGE analysis (Coomassie stain). Due to the increased sensitivity of the T356D annexin VI to proteolysis during storage, protease inhibitors were added during the final steps of isolation.

Protein concentrations were determined by the method of Bradford (*11*) or UV absorption at 276 nm using a molar absorption coefficient for annexin VI of 41,180 M^{-1} cm^{-1} and a molecular mass of 70 kDa.

Liposome and Protein Self-Aggregation Assays. Aggregation of bovine brain liposomes (Sigma product B1502, containing 50% phosphatidylserine) was followed by monitoring the changes in absorbance at 350 nm in a Beckmann DU70 recording spectrophotometer. Assays were carried out for 10 min in 1 cm quartz cuvettes at room temperature in a buffer containing 20 mM Hepes (pH 7.4), 0.5 mM $MgCl_2$, 10 μg of protein, and various concentrations of free calcium. The assay was initiated by addition of liposomes to a final concentration of 10 μM.

Protein self-association was similarly measured by following the changes in turbidity at 350 nm. Increasing

[1] Abbreviations: T356D, Thr-356 → Asp site-directed mutant; EGTA, ethylene glycol bis(β-aminoethyl ether)-*N*,*N*,*N*′,*N*′-tetraacetic acid; HEPES, *N*-(2-hydroxyethyl)piperazine-*N*′-2-propanesulfonic acid; Tris-HCl, tris(hydroxymethyl)aminoethane; PBS, phosphate-buffered saline; SDS−PAGE, sodium dodecyl sulfate−polyacrylamide gel electrophoresis.

amounts of calcium were added to 10 μg of protein in 20 mM Tris-HCl (pH 7.4), and absorbance was measured at 350 nm. The curves were corrected by subtracting the absorbance at 0 M calcium.

Fluorescence Measurements. Fluorescence measurements were taken using a SPEX Fluorolog spectrofluorimeter. Tryptophan excitation was at 280 or 295 nm with emission spectra recorded from 300 to 380 nm. Protein solutions were approximately 0.1 mg/mL in 20 mM Tris-HCl (pH 7.4). Spectra were generally accumulated over three scans with a step width of 1 nm/s, corrected for the solvent background, and normalized at maximum fluorescence emission.

An increase in fluorescence emission intensity at 353 nm for the wild-type and T356D annexin VI was used to monitor calcium binding in the absence or presence of phospholipids. For these measurements, calcium was added in small aliquots from a concentrated stock. Intensity differences at 353 nm ($I - I_o$) were taken from normalized spectra and plotted as Hill plots in a semilogarithmic fashion. The resulting binding curves were fitted using the nonlinear regression function of GraphPad Prism version 3.02 for Windows (GraphPad Software). Acrylamide quenching was detected by adding increasing amounts of acrylamide from a 5.7 M stock solution to the protein samples. Stern−Volmer quenching constants were calculated from least-squares fits to Stern−Volmer plots corresponding to the intensity at 353 nm.

For urea denaturation experiments, 0.1 mg/mL protein was incubated with various amounts of a freshly prepared urea solution overnight at 25 °C. Fluorescence emission was monitored at 362 nm. When a two-state character of the unfolding of annexin VI was assumed, the values for $[D]_{1/2}$ (concentration of the denaturant where 50% of the protein is unfolded) and $\Delta G°_{N-D}$ (free energy of unfolding in the absence of denaturant) were determined by the linear extrapolation method (*12*).

Analytical Trypsin Digest. Analytical trypsin digests were performed by incubating 1 μg of protein with 0.05 μg of trypsin in 0.1 M ammonium bicarbonate (pH 8.5). The reaction was stopped by adding SDS sample buffer and heating to 100 °C for 2 min. Samples were taken after 0, 10, 30, and 60 min and analyzed by standard SDS−PAGE. After SDS−PAGE, the protein bands were electroeluted onto a PVDF membrane (ProBlott, Applied Biosystems) according to the manufacturer's instructions and stained with Coomassie Blue. N-Terminal (Edman) sequencing was then was performed on an Applied Biosystems Procise protein sequencer (Biomolecular Research Facility of the University of Virginia) to identify the trypsin cleavage sites.

Nondenaturing Polyacrylamide Gel Electrophoretic Analysis. Samples of wild-type annexin VI and T356D were analyzed in polyacrylamide gels in the absence of SDS. For a range of acrylamide concentrations from 5 to 13%, separate gels were prepared and electrophoresis was performed in a buffer consisting of 50 mM Tris-HCl (pH 8.3) and 5 mM EGTA; 30 μg of both wild-type and T356D annexin VI were applied in each gel, and all gels from one set of experiments were run at 40 mV for 4 h simultaneously. Calculation of the coefficient of retardation from the mobility of the different proteins was achieved by plotting values for migration against concentrations of polyacrylamide. The slopes of the linear regression of the resulting Ferguson plot represent the coefficients of retardation (*13*).

Circular Dichroism and Thermal Denaturation Experiments. CD spectra were recorded on an AVIV 215 CD spectrometer (AVIV Instruments) equipped with CDS software for automated data acquisition and processing. Quartz cells of with an optical path length of 0.1 cm and protein concentrations of 0.3 mg/mL in NaCl/P_i (140 mM sodium chloride, 4 mM sodium phosphate, and 1.5 mM potassium phosphate) with 1 mM EGTA or 2 mM free calcium were used.

Melting curves for wild-type annexin VI and T356D were recorded by monitoring changes in the dichroic intensities at 222 nm. For thermal denaturation experiments in the range of 20−80 °C, a heating rate of 1 °C/min was applied with an equilibration time of 2 min at each temperature. Thermodynamic parameters were determined by global fitting of the unfolding profiles according to the Gibbs−Helmholtz equation using the nonlinear regression analysis program KaleidaGraph (version 3.0, Synergy Software, PCS Inc., for Macintosh).

Crystallographic Analysis of T356D. Recombinant T356D annexin VI was crystallized at room temperature by the hanging drop method. The reservoir composition was 0.5 M sodium acetate buffered with 0.1 M imidazole (pH 7.4). Seven microliters of the protein solution (15−20 mg/mL) was mixed with 3 μL of the reservoir to prepare the hanging drop. Although neither calcium nor EGTA was added, the free calcium concentration in the buffer combination used for the crystallization drop was 4 μM (in the absence of protein) as measured with a calcium sensitive electrode. Crystals appeared after 2 days and grew to a maximal size of 0.1 mm × 0.1 mm × 0.5 mm. Attempts to crystallize T356D annexin VI in the presence of up to 0.5−1 mM calcium resulted only in heavy microcrystalline precipitation in the crystallization droplet, while soaking calcium-free crystals in mother liquor containing 1 mM calcium caused cracking of the crystals as reported for wild-type annexin VI (human) (*5*).

X-ray diffraction was assessed using synchrotron radiation (λ = 0.971 Å) at the Brookhaven National Laboratory Synchrotron, beamline X4A, to 2.50 Å resolution. Prior to data collection, crystals were flash-frozen in liquid nitrogen after soaking in mother liquor with 35% ethylene glycol as a cryoprotectant and kept at that temperature during the measurement. One degree oscillation frames were acquired on image plates and scanned by a Fuji scanner. Data were reduced and scaled using HKL2000 and SCALEPACK (*14*).

The structure was determined by molecular replacement, using the coordinates of human wild-type annexin VI as a model. Crystals of T356D were found to be isomorphous with the *P*4(3) crystals of both human wild-type annexin VI and bovine annexin VI. Molecular replacement and refinement were performed using CNS-SOLVE (*15*). Model building was carried out in O (*16*). Cycles of rebuilding, refinement, and calculation of difference and simulated annealing omit maps improved the model to its final form. Data collection and refinement statistics are listed in Table 1.

RESULTS

Crystallographic Analysis of T356D Annexin VI. Comparison of the T356D and wild-type annexin VI structures shows that the overall conformations of the molecular

Table 1: Crystallographic Data and Refinement Statistics for the Structure Solution of T356D

crystallographic data	
space group	*P*4(3)
cell dimensions	$a = 67.97$ Å, $b = 67.97$ Å, c = 204.6 Å, $\alpha = \beta = \gamma = 90°$
resolution range (Å)	50−2.5
no. of unique reflections	32036
completeness (%) (highest-resolution shell)	97.2 (99.7)
R_{merge}	0.089
model refinement	
applied resolution limit (Å)	2.65
no. of reflections used in refinement	26029
no. of non-H atoms	5264
no. of calcium ions	5
no. of water ions	148
R_{cryst}	0.225
R_{free}	0.279
rmsd for bond lengths (Å)	0.006901
rmsd for angles (deg)	1.23886
average *B* factor (Å^2)	42.8

structures are quite similar. The two core domains, A and B, in T356D are found in the same perpendicular orientation as in the wild-type structures of (calcium-free) human annexin VI (*5*) and (calcium-containing) bovine annexin VI (*6*) (Figure 1). The root-mean-square deviation for the backbone in core A is 0.74 Å and for that in core domain B 0.80 Å. The root-mean-square deviation in the linker region where the mutation occurs is 0.71 Å for the complete length of the linker (residues 320−360) and only 0.39 Å for residues 340−360.

At the site of the mutation, additional electron density is found reflecting the presence of the introduced aspartate residue. The protein circumvents steric clashes and negative repulsion of the larger side chain and the additional negative charge by flipping the carbonyl oxygen of the nearby Cys-669 by 180°, inducing conformational changes in the subsequent C-terminal residues as shown in Figure 1B and reflected by the changes of the values for ϕ and ψ (Cys-669, −48.94° and 151.76° for T356D vs −40.26° and −55.12° for the wild type, respectively). By adjustment of the five C-terminal residues, the protein structure is able to accommodate the changes introduced by the mutation without further conformational rearrangements of the connector region.

However, some conformational changes are evident in one of the calcium-binding loops in the T356D structure (Figure 2). A−B loop V (i.e., between the A and B helix V) is in a

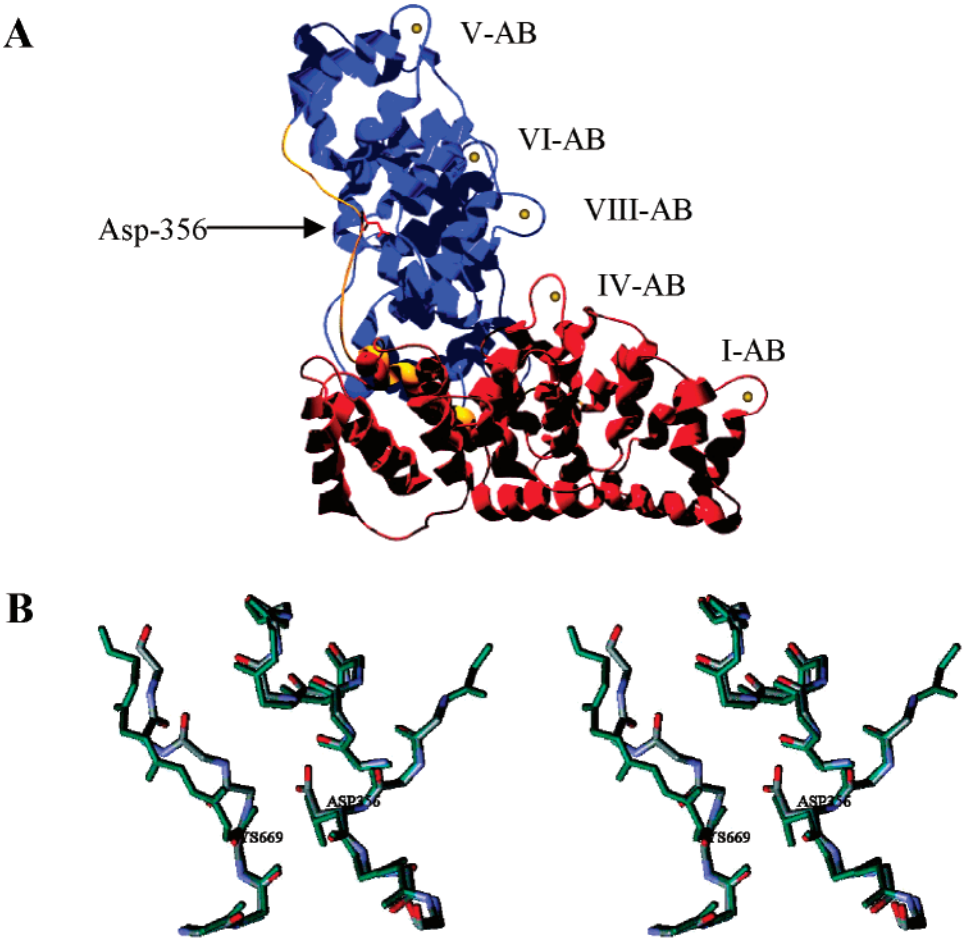

FIGURE 1: (A) Ribbon representation of the T356D annexin VI structure determined in this study. Bound calcium atoms are represented as yellow balls, and the binding loops are labeled. Asp at position 356 in the interlobe connector region (orange) is presented as a stick model in red. Core domain A is in red and core domain B in blue. (B) Stereoview of the site of mutation T356D. The wild-type annexin VI molecule in green is overlaid with T356D in gray with carbonyl and carboxyl oxygens in red. The backbone carboxyl group of Cys-669 of the interacting C-terminal fragment of the molecule is flipped over by 180° in the T356D structure to circumvent sterical clashes by the introduced aspartate. This figure was generated using Swissprot PDB Viewer (*34*).

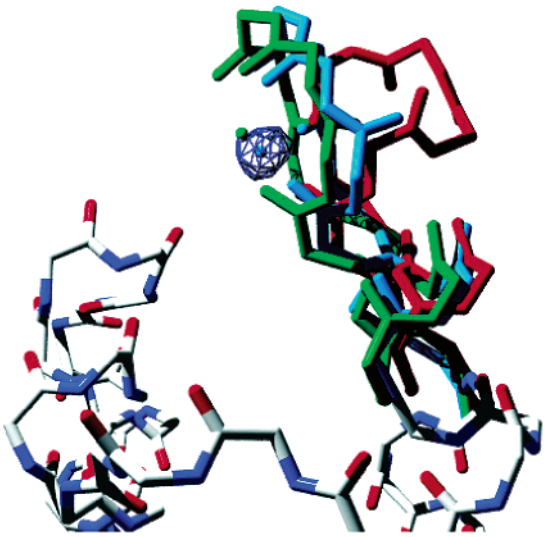

FIGURE 2: A−B loop V has a conformation in the calcium-bound annexin VI structure significantly different from that in the calcium-free annexin VI. Blue represents T356, and the electron density difference ($F_o - F_c$) map for the bound calcium atom is contoured at 3σ. Green represents the calcium-containing bovine annexin VI structure. Red represents human wild-type annexin VI without calcium.

Table 2: Calcium-Binding Loops Occupied by Calcium in the Crystal Structure of T356D[a]

loop	residues	sequence 1	2	3	4	mean Ca−O distance (Å)
I A−B	33−37, 77	**M** K	**G** F	**G** S	**E***	2.38
VI A−B	264−270, 308	**M** K	**G** L	**G** T	**D****	2.26
V A−B	376−382, 420	**M** K	**G** L	**G** T	**E****	2.38
VI A−B	448−454, 492	**M** E	**G** A	**G** T	**D***	2.10
VIII A−B	612−618, 656	**M** K	**G** A	**G** T	**D***	2.35

[a] Bold residues are conserved Met, Gly, Gly, and Asp/Glu residues involved in calcium binding. The numbers 1−3 represent carbonyl main chain oxygens, and the number 4 represents a carboxylate group from either aspartate of glutamate with one asterisk marking unidentate and two asterisks bidentate carboxylates. No water ligands with high occupancy are observed in the calcium coordination sphere.

more open conformation than in the crystal structure of the human wild-type structure and resembles more the conformation of the corresponding A−B loop V in the bovine calcium-containing structure as depicted in Figure 2. Interestingly, this putative calcium-binding loop and four other calcium-binding sites are occupied by calcium ions in the T356D structure despite crystallization in the presence of only residual amounts of free calcium (4 μM). The calcium-containing bovine annexin VI structure was determined in the presence of 600 μM free calcium (*6*). Other calcium-bound annexin structures have usually been determined with millimolar amounts of total calcium in the crystallization medium (*17*−*19*).

While the human wild-type structure has no calcium molecules present in the crystal structure, the densities for the five calcium ions in the T356D structure are coordinated in a similar manner compared to the coordination of calcium in the bovine annexin VI structure (Table 2). The five A−B loops occupied in T356D annexin VI belong to the high-affinity type II calcium-binding sites (*20*), while the D−E binding loop at Trp-192 which is also occupied in the bovine crystal structure but is empty in our structure belongs to the

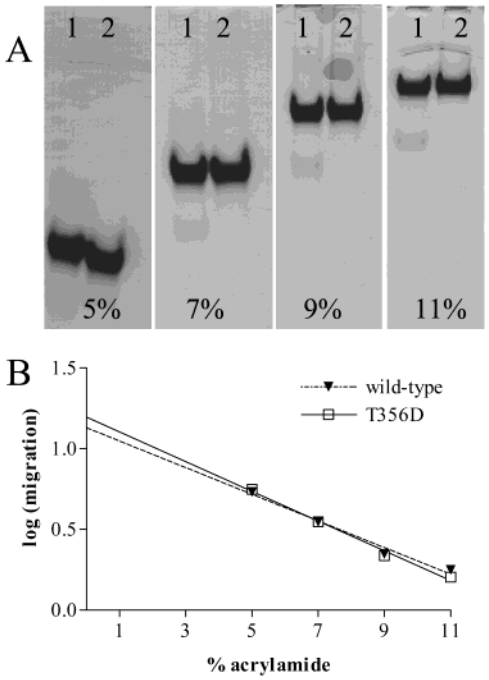

FIGURE 3: (A) Native gel electrophoresis of annexin VI: lane 1, wild-type; and lane 2, T356D. Each panel represents a single gel run at a distinct polyacrylamide concentration under native conditions. Gels were run for 4 h at 40 mV and stained with Coomassie Blue. Thirty micrograms of protein was applied to each gel lane. (B) Ferguson plot representation of the migration of each protein at different polyacrylamide concentrations. The slope of linear Ferguson plots is proportional to the square of the particle size. The intercept on the ordinate specifies the particle-free mobility. In general, particles similar in size or mass have parallel Ferguson plots. Particles with the same net charges have the same intercept on the log(migration) axis (ordinate). The wild type and T356D have slightly different net charges due to the T → D substitution and therefore different intercepts at the ordinate. The nonparallel slopes indicate different shapes, as the molecular masses are virtually the same.

low-affinity type III class. Apparently, with the small calcium amounts in our experiment, only high-affinity binding sites are occupied.

Electrophoretic Mobility of Wild-Type Annexin VI and T356D under Nondenaturing Conditions. Native gel electrophoresis was performed on T356D and wild-type annexin VI to assess different migration properties of the two protein variants. Because retardation of proteins by polyacrylamide is dependent on both the net charge and the particle size and shape, this method can be utilized to detect differences in native conformations (*13*). Figure 3A shows native polyacrylamide gels probing the migration properties of the wild type and T356D at different polyacrylamide concentrations (5−11%). It is clearly visible that T356D migrates faster than the wild-type protein at low polyacrylamide concentrations due to the additional charge introduced by the T → D mutation. On the other hand, T356D migrates more slowly than the wild type at high polyacrylamide concentrations, implying a more extended shape in comparison to the wild-type protein since the molecular masses of the two proteins are virtually the same. Evaluation of the resulting Ferguson plots (Figure 3B) for both proteins shows an 11% higher coefficient of retardation for T356D annexin VI. It has been shown previously that there is a linear correlation between the square root of the coefficients of retardation and the

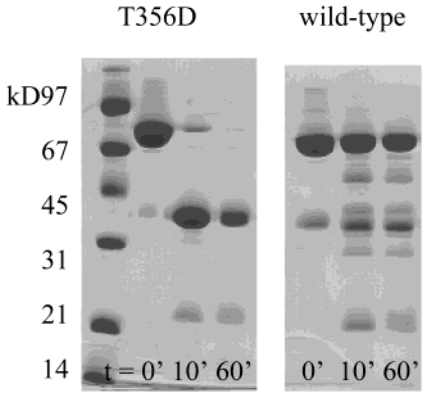

FIGURE 4: Proteolytic digest of wild-type and T356D annexin VI. The experimental procedures are described in Materials and Methods. Ninety percent of T356D (70 kDa) is cleaved into fragments corresponding to the two core domains (35 kDa) at two trypsin cleavage sites in the linker region after incubation for 10 min at 37 °C. The wild type is less susceptible to cleavage. After incubation for 1 h, 80% full-length protein can be detected.

geometrical mean radius of protein molecules. In this context, it can be concluded that T356D exhibits a greater mean radius than wild-type annexin VI.

Proteolytic Analysis. Analytical trypsin digest experiments were used to probe for differences in the susceptibility of T356D to proteolytic degradation. Proteolytic cleavage was followed for 60 min, and the products were visualized by SDS−PAGE and Coomassie Blue staining. While Figure 4 shows ~80% of the full-length (70 kDa) wild-type protein remaining after incubation with the protease at 37 °C for 30 min, 90% of T356D was cleaved into products of half the size (ca. 35 kDa) within the first 10 min. Experiments performed in a calcium-free medium or in the presence of 2 mM calcium gave similar results. N-Terminal sequencing of the product bands revealed two trypsin cleavage sites near Asp-356, the site of mutation: Lys-354 and Arg-350.

Intrinsic Fluorescence Properties of T356D and Wild-Type Annexin VI. In a calcium-free environment, annexin VI has a broad fluorescence emission maximum in the range of 320−330 nm upon excitation at 280 nm. Two tryptophan residues located in different microenvironments in the molecule (Figure 5A) contribute primarily to an emission maximum at 324 nm for the wild-type protein and one at 325 nm for T356D (Figure 5B). Emission maxima for excitation at 295 nm are at 330 nm for the wild type and T356D (not shown).

Upon addition of 1 mM calcium in the absence of phospholipids, a decrease in intensity was observed. This behavior has also been reported for annexin V (*21*). However, we attribute this decrease in fluorescence emission intensity to self-association of the protein rather than solvent quenching of the tryptophan residues since a visible protein precipitate was formed with increasing calcium levels. For this reason, all recorded spectra were normalized to their emission maximum values. Both proteins exhibit a red shift of their normalized emission maximum in the presence of calcium to 335 nm for wild-type annexin VI and 337 nm for T356D. In addition, a relative increase in the intensity at 353 nm is observed that is 24% more pronounced in T356D (Figure 5B).

On the other hand, fluorescence emission spectra in the presence of calcium and phospholipid vesicles are similar for the wild-type and T356D (Figure 5C). The emission maxima are red shifted to 338 nm with a relative increase in the emission intensity at 353 nm for both proteins which is similar to the increase at 353 nm observed for calcium-containing T356D in the absence of phospholipids as seen in Figure 5B.

The accessibility of the buried Trp-343 was analyzed by polyacrylamide quenching (Figure 5D). The Stern−Volmer quenching constant $K_D[Q]$ for wild-type annexin VI is 3.58 ± 0.21 M^{-1}, while quenching of T356D annexin VI results in a higher value of 5.38 ± 0.17 M^{-1}, indicating a higher degree of exposure of the buried Trp-343 in T356D.

Calcium Binding. Since the crystallographic analysis of T356D revealed five calcium-binding sites occupied at the low concentration of calcium present in the crystallization setup, calcium binding studies were performed to compare the binding properties of T356D and wild-type annexin VI. The changes in intrinsic fluorescence emission at 353 nm upon calcium addition in the absence of phospholipids were utilized to characterize calcium binding (Figure 6).

Titration of wild-type annexin VI with calcium results in a sigmoid binding curve with a K_D value of 250 μm. The Hill coefficient under the conditions of the experiment is 3.48, indicating substantial cooperativity leading to the observed change in tryptophan fluorescence upon calcium binding. On the other hand, the curve for T356D denotes less or no cooperativity with a Hill coefficient of 0.97, while the K_D value is 20% lower (204 μm) than for wild-type annexin VI.

Solvent-Induced and Thermally Induced Unfolding of Wild-Type Annexin VI and T356D. Urea unfolding curves of wild-type and T356D annexin VI show a typical sigmoid shape with one inflection point indicating a two-state transition of unfolding (Figure 7A). For this reason, the linear extrapolation method was used for evaluation of the urea denaturation curves (*12*). The two unfolding profiles clearly show a higher resistance of the wild-type protein toward urea with a 3 times lower midpoint of denaturation ($[D]_{1/2}$) for T356D. Table 3 summarizes the thermodynamic parameters of the unfolding experiments.

Temperature-induced unfolding of T356D and wild-type annexin VI occurs as a two-state transition from the α-helical native state to a denatured state (Figure 7B). CD spectra of the denatured states of both proteins are characterized by a significant loss in secondary structure at 80 °C (not shown). Thermal denaturation was followed by monitoring changes in the dichroic intensities at 222 nm upon heating. In the absence of calcium, the T_m values differ significantly for the wild type and T356D, with an 8.0 K lower melting temperature for T356D annexin VI. In the presence of 2 mM calcium, the T_m value of T356D is not significantly changed, while it is reduced by 1.2 K for the wild type. It is interesting that in the presence of calcium the post-transition slope for both proteins is less steep than under calcium-free conditions, while the transition slopes are steeper for the calcium-bound protein forms. This could indicate a more cooperative unfolding pathway and a more compact set of denatured states due to calcium binding.

ΔH_m values were determined by global fitting using the Gibbs−Helmholtz equation and are similar for T356D and the wild type in the absence and presence of calcium.

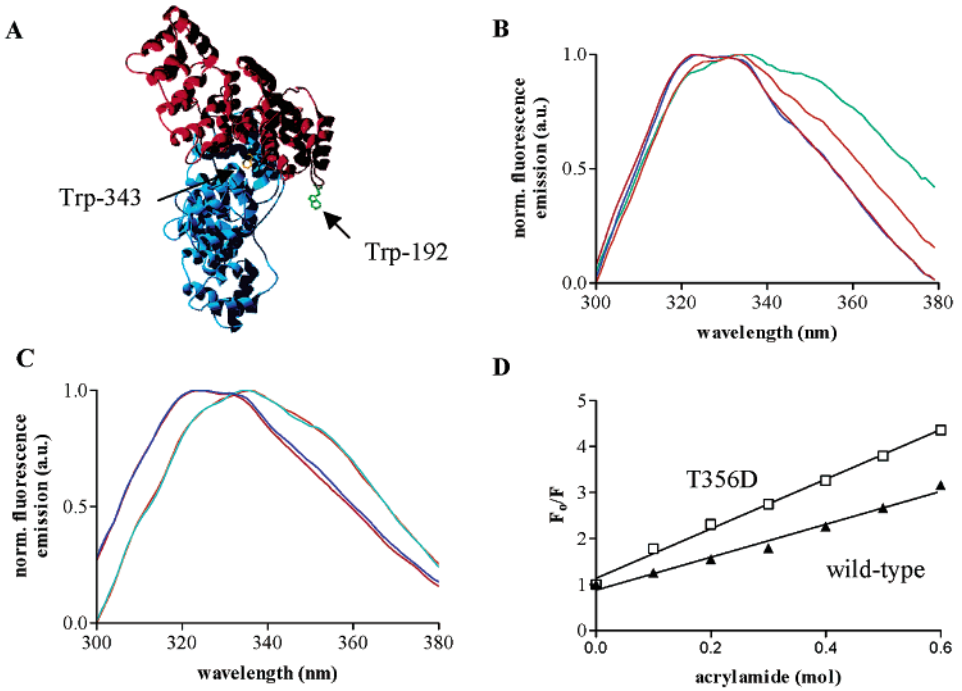

FIGURE 5: (A) Ribbon representation of human annexin VI. Note that Trp-192 in core domain A is completely exposed to solvent in the crystal structure (with and without calcium), while Trp-343 in core B is buried in an interdomain pocket. Changes in fluorescence emission should therefore arise mainly from changes in the tertiary structure around Trp-343. (B) Fluorescence emission spectra of the wild type (red, without calcium; orange, with 1 mM calcium) and T356D (dark blue, without calcium; light blue, with 1 mM calcium). While spectra with excitation at 280 nm are very similar in a calcium-free environment, a red shift occurs upon calcium binding. A pronounced shoulder emerging at 353 nm in the case of T356D indicates a large contribution of Trp-343 becoming exposed to solvent in the presence of calcium. (C) Fluorescence emission spectra of the wild type (red, with phospholipids and without calcium; orange, with phospholipids and 20 μM calcium) and T356D (dark blue, with phospholipids and without calcium; light blue, with phospholipids and with 20 μM calcium). The spectra of the calcium-containing protein samples are very similar but resemble more the calcium-containing lipid free emission profile of T356D from Figure 5B. (D) The Stern−Volmer plots of acrylamide quenching of the fluorescence signal at 353 nm gives a quenching constant (K_D[Q]) of 3.58 ± 0.21 M^{-1} for the wild type and 5.38 ± 0.17 M^{-1} for T356D, indicating a higher level of exposure of the buried Trp-343 in T356D.

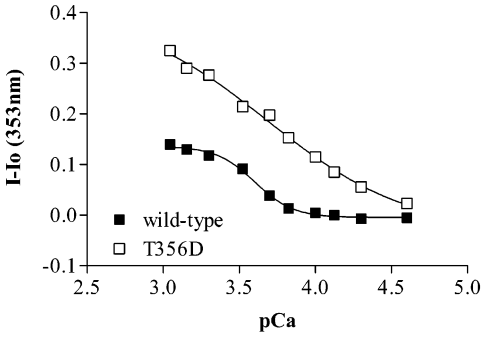

FIGURE 6: Calcium titration curves of the two proteins followed by the increase in fluorescence emission intensity at 353 nm. Curves are represented in a semilogarithmic fashion and fitted with a nonlinear regression curve fit program (GraphPad Prism version 3.02 for Windows, GraphPad Software). T356D loses the cooperative behavior of calcium binding with a Hill coefficient of 0.97 in contrast to a Hill coefficient of 3.48 for the wild-type protein.

Interactions with Membranes. While Bandorowicz-Pikula and Pikula reported aggregation of phospholipid vesicles in the presence of calcium by annexin VI (*22*), other studies do not confirm this behavior (*23*), and a possible regulatory role of annexin VI as an inhibitor of membrane fusion has been proposed (*24*). While probing the interaction of wild-type annexin VI and T356D with 50% phosphatidylserine vesicles, we could not detect a significant level of calcium-induced lipid aggregation for either the wild type or T356D at calcium concentrations of up to 3 mM. However, as in our fluorescence studies, we did observe an increased level of self-association of T356D in the presence of calcium compared to that for the wild type (Figure 8) as judged from an increase in the absorbance of the protein sample without phospholipids at 350 nm upon titration with calcium. The extent of self-aggregation of T356D is 60% greater than that of wild-type annexin VI at the highest calcium concentrations. This self-association of annexin VI in the presence of calcium could possibly hinder its ability to promote membrane aggregation.

DISCUSSION

T356D as a Model for Phosphorylated Annexin VI. Phosphorylation-mimicking mutations have been successfully used in several studies of annexins to evaluate the impact of phosphorylation on membrane aggregation and binding properties. Mutagenic substitution of Ser-21 with aspartate in annexin I, for example, faithfully reproduces the effects of phosphorylation by protein kinase C at this site on the ability of annexin I to aggregate chromaffin granules in a calcium-dependent fashion (*25*). The same holds true for annexin IV where replacement of Thr-6 with aspartate was shown to have an inhibitory impact on liposome aggregation identical to that of in vitro phosphorylation (*17*).

Annexin VI has two putative phosphorylation sites (Ser-13 and Thr-356); Thr-356 is located in the N-terminal portion of core domain B that is connected to core domain A through a flexible linker region that includes this site. Electron

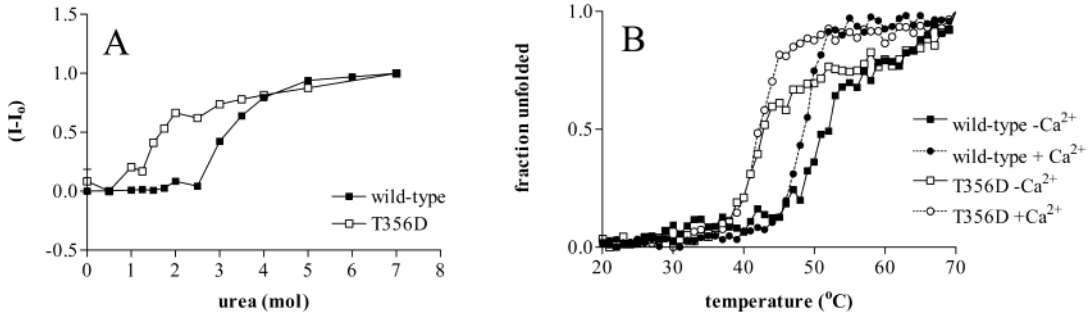

FIGURE 7: (A) Urea-induced unfolding of the wild-type annexin VI and T356D followed by changes in the fluorescence intensity at 362 nm. Unfolding parameters were determined by the linear extrapolation method (*12*) assuming a two-state unfolding transition and are listed in Table 3. (B) Thermally induced unfolding of the two proteins in the presence and absence of 1 mM calcium. Thermodynamic parameters were determined by global fitting of the unfolding profiles according to the Gibbs−Helmholtz equation using the nonlinear regression analysis program KaleidaGraph (version 3.0, Synergy Software, PCS Inc. for Macintosh) and are listed in Table 3.

Table 3: Unfolding Parameters for the Solvent-Induced and Thermally Induced Denaturation of Wild-Type Annexin VI and T356D Determined by the Linear Extrapolation Method (*12*) for Urea Unfolding and Global Fitting According to the Gibbs−Helmholtz Equation for the Thermal Denaturation Curves

thermal unfolding	ΔH_m (kJ/mol)	T_m (K)	ΔT_m (K)
wild type in EGTA	139.23 ± 25.34	322.91 ± 0.33	−
wild type in 2 mM Ca^{2+}	155.08 ± 9.93	321.56 ± 0.11	−1.35
T356D in EGTA	150.06 ± 11.85	314.41 ± 0.30	−8.50
T356D in 2 mM Ca^{2+}	149.89 ± 24.35	315.17 ± 0.14	−7.74

urea unfolding	$\Delta G°_{N-D}$ (kJ/mol)	$[D]_{1/2}$(urea) (M)	m (kJ mol^{-1} M^{-1})
wild type in EGTA	16.96 ± 1.754	3.40	4.98 ± 0.54
T356D in EGTA	13.43 ± 1.423	1.74	7.72 ± 0.92

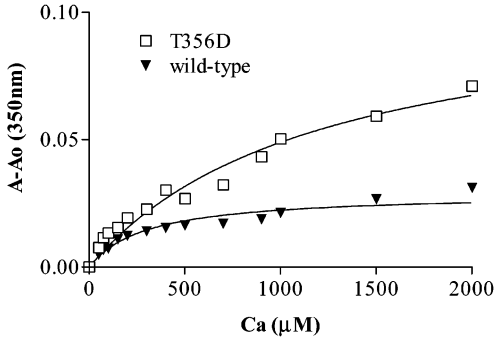

FIGURE 8: Self-association of T356D and wild-type annexin VI was monitored by changes in the absorbance at 350 nm with increasing concentrations of calcium.

microscopic studies show that this linker region is sufficiently flexible that the two core domains can adopt parallel or antiparallel conformations upon membrane binding (*7*).

Although the similarity of the sequence environment near Thr-356 to known phosphorylation sites in other annexins provides a strong rationale for studying the effects of mutation at this site, the physiological circumstances under which this residue may be phosphorylated are not well characterized. Moss et al. (*8*) demonstrated that annexin VI is phosphorylated on serine and threonine in a slow, growth-dependent manner in fibroblasts, and canonical sites Ser-13 and Thr-356 would seem to be likely candidates for the relevant sites. However, the specific threonine that underwent phosphorylation was not mapped. Both Ser-13 and Thr-356 are found within sequence motifs that are recognized by protein kinase C, and in vitro studies have demonstrated that annexin VI can be phosphorylated by protein kinase C, but at a slow rate compared to annexin I, which is an excellent protein kinase C substrate (*26*). The slow rate may be due to the fact that the basic residue downstream from Ser-13 is a histidine rather than a lysine or arginine, and the possibility that it may be difficult to displace Thr-356 from its sheltered pocket between the two annexin domains to allow the kinase access. More rapid phosphorylation of a 68 kDa protein that may be annexin VI is seen when calcium-dependent membrane-binding proteins are incubated with chromaffin granules (*27*), when membranes of placental syncitiotrophoblasts are incubated in vitro (*28*), or when detergent extracts of neutrophils are incubated in vitro (*29*). In these in vitro experiments, however, the kinases that are involved are unknown, and again the sites of phosphorylation have not been mapped.

In preliminary experiments, we confirmed that annexin VI can be phosphorylated in vitro at a slow rate compared to annexin I by protein kinase C (unpublished observations). Anticipating that the T356D mutation might be useful for demonstrating that this residue is responsible for some or all of this phosphorylation, we also attempted to phosphorylate T356D annexin VI with protein kinase C in parallel experiments. Surprisingly, T356D undergoes net phosphorylation to an extent several times greater than that of the wild type. Since Thr-356 is not present, other phosphorylation sites must be involved in this enhanced phosphorylation. This result suggests the interesting possibility that the conformational and dynamic changes that we have demonstrated are associated with the mutation cause additional sites to become available for phosphorylation. Possibly, in vivo phosphorylation of Thr-356 could serve to initiate a cascade of phosphorylation events at other sites. Clearly, the details of annexin VI phosphorylation in vitro and in vivo warrant further investigation.

Crystal Structure of T356D. The only previous report of the structure of a phosphorylation-mimicking mutant of an annexin comes from Kaetzel et al. (*17*), who substituted Thr-6 with Asp in the N-terminal domain of annexin IV. This site corresponds to Thr-356 in annexin VI. Crystals of T6D are isomorphous to the wild-type crystals, and the two molecular structures are quite similar with a root-mean-square deviation of only 0.38 Å. The only difference appears in the flexible N-terminal region where the introduction of a negatively charged aspartate causes the N-terminal strand to be released from its anchored position in the wild-type

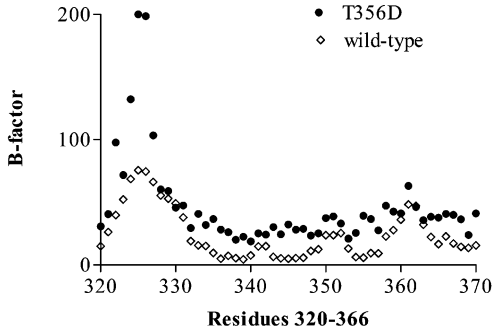

FIGURE 9: Comparison of the *B* values of wild-type and T356D annexin VI in the flexible linker region (residues 320−370). High *B* values occur for residues 324−326 and 328 in the T356D structure.

crystal structure, whereas the core domain of annexin IV is unchanged.

The crystal structure of T356D determined in this study at 2.65 Å resolution shows no significant change in the relative orientation of the core domains A and B, and the linker region remains in close contact with the core domains. In the case of annexin IV, there are only three hydrophobic interactions at Thr-6, Val-7, and Phe-13 anchoring the N-terminal region to the core of annexin IV, so it is not surprising that the N-terminus of annexin IV is much more flexible than the connector region in annexin VI where an extensive area of contacts involving the two core domains and the connector segment (3340 Å^2) (*6*) would need to be destabilized by the introduced negative charge to free the connector region. Although a release of the linker region from the core domain is not observed in the crystal structure, high *B* values for residues 324−326 and 328 at the A domain side of the linker may indicate a higher flexibility of this region of the protein (Figure 9).

The overall similarity of the structures of the wild-type protein and T356D might also be explained by the formation of strong crystal contacts under the conditions of the crystallization experiment that favored the original wild-type conformation with Asp-356 anchored toward the core domain, while different more flexible conformations might not be preferred under these conditions.

Although the core domains are in a similar relative orientation, a major difference between the T356D and wild-type crystal structures can be seen in the calcium-binding sites. Five of the six known calcium-binding loops are occupied in T356D. Only the high-affinity binding sites of class II were found to harbor calcium. Previously, wild-type annexin VI was crystallized in a calcium-free form (*5*) in which no calcium-binding sites were found to be occupied in the crystal structure at 3.2 Å resolution. The calcium-containing form of the wild-type protein was determined by Avila-Sakar et al. (*6*) at 2.9 Å, revealing the presence of six calcium-binding loops occupied in the presence of 600 μM calcium. Our T356D structure at 2.65 Å resolution clearly shows the presence of five calcium atoms and a conformational change in A−B loop V equivalent to that in the calcium-containing structure. Although the free calcium concentration in the crystallization medium was only 4 μM, it is not easy to assess how much calcium was carried by the protein through the last steps of purification in the absence of EGTA. It is also known that during the vapor diffusion crystallization processes concentrations can vary in the crystallization droplet over the time of crystal formation. On the other hand, crystallization of T356D was carried out under the same conditions that were used for the wild-type protein where no calcium can be detected in the structure. Thus, it appears that T356D exhibits a higher affinity for calcium.

Mani and Kay (*30*) determined a K_D value for calcium binding for native annexin VI in solution of 20 μM using fluorescence studies with the TNS-labeled protein, while Moore et al. (*31*) determined a K_D value of 0.4 μM. However. our experiments resulted in much higher K_D values for wild-type annexin VI. Mani and Kay also found only one class of calcium-binding sites in contrast to the two classes determined by X-ray crystallography. The differences between our results from previous reports could come from the limitations of the use of a noncovalent hydrophobic probe like TNS that could affect calcium binding itself. On the other hand, the changes in fluorescence emission in our experiments may well reflect only the lower-affinity sites.

However, our measurements of the changes in the intrinsic fluorescence of the protein seem to reveal different modes of calcium binding for wild-type annexin VI and T356D. The calcium titration curve for T356D lacks the cooperative behavior observed for the wild-type protein. We speculate that the relative spatial arrangement of the calcium-binding sites might be affected due to the mutation, resulting in the loss of cooperativity of calcium binding in a more flexible and extended protein molecule.

Conformation in Solution. Despite the similar crystal structures of wild-type annexin VI and T356D, the dynamic and fluorescence properties of the two proteins indicate that the mutation causes an altered conformation in solution. It has been suggested that variations in the membrane aggregation activities of phosphorylated forms and phosphorylation-mimicking mutants of other annexins can be attributed to conformational changes in the N-terminal domains (*17*, *25*, *32*). Evidence for a similar conformational change in the linker region of annexin VI upon mutation comes first from a comparison of the retardation coefficients in gel electrophoresis that indicate a more extended shape of T356D.

In addition, T356D was found to be more sensitive to proteolytic degradation than the wild-type protein. This again suggests that the negative charge introduced into the linker region may induce a conformational flexibility in this part of the molecule, which results in a release of the linker from the domain B core. This finding is in agreement with studies of other annexins where phosphorylation-mimicking mutations result in an increased proteolytic susceptibility in the N-terminal region (*17*, *25*, *32*).

Moreover, fluorescence studies were used to obtain additional information about the environment of Trp-343, a residue in the linker region that is buried in a pocket in core domain B. As Trp-192 of annexin VI is already solvent-exposed in either the calcium-free or calcium-bound form of annexin VI (as seen from the crystal structures), calcium-induced changes in the fluorescence properties of annexin VI should mainly emerge from conformational changes around Trp-343.

While a decrease in fluorescence intensity upon addition of calcium appears to come from self-aggregation of both proteins as judged from the appearance of a precipitate in

the fluorescence cuvette, the normalized spectra with a red-shifted maximum at 337 nm and an emerging shoulder at 353 nm indicate greater exposure of Trp-343 to solvent and thus a more flexible conformation around this residue. Although this behavior can be observed for the wild-type protein to some extent, there clearly is more pronounced exposure of the buried Trp-343 at high calcium concentrations in T356D. In this sense, the mutation, and by inference phosphorylation, appears to alter the structure of the protein in a manner similar to that of calcium binding; this is also evident from the fluorescence spectra in the presence of phospholipids and calcium. Thus, phosphorylation may be a means of enhancing the calcium sensitivity of annexin VI. This would be consistent with the higher level of occupation of the calcium-binding sites in the T356D crystal structure.

To assess this more pronounced flexibility in case of T356D, we performed thermal and chemical denaturation experiments. Little is known about the thermodynamic stability of phosphorylation-mimicking mutants of annexins in general. Although the overall energy of unfolding (ΔG_o) does seem to be slightly affected by the mutation, the $[D]_{1/2}$ value for urea denaturation and the melting temperature are dramatically decreased in T356D. While the slopes of the thermal denaturation curves are very similar for T356D and the wild-type protein, the *m* value for urea denaturation is higher for T356D. The *m* value reflects the hydrophobic accessible surface area exposed during a chemically induced unfolding experiment (*33*). This could indicate that the surface area of T356D accessible to the denaturant is higher due to looser contacts and an increased flexibility of the two core domains. We also interpret the higher melting temperature of the wild-type protein as an indication of stronger contacts between the core domains that need to be weakened before the secondary structure is unfolded. Interestingly, the addition of calcium results in a more compact set of unfolded states, as judged from the less steep post-transition portion of the unfolding curve, suggesting stabilization of the unfolded state by calcium.

CONCLUSION

It is a limitation of structure determination by X-ray crystallography that only a snapshot of a single conformation is typically obtained. In the case of T356D, crystallography yields only a limited insight into the dynamic changes that may take place upon phosphorylation. Our solution data show that much larger conformational changes occur in solution due to the mutation. These changes appear to correspond to changes implied in the case of the N-terminal phosphorylation of other annexins. The changes may enable annexin VI to interact with one or more membranes in far more complex manners than could be inferred from the crystallographic structure alone. We conclude that phosphorylation is likely to be a critical determinant of the range of functions annexin VI performs in vivo.

ACKNOWLEDGMENT

We thank Sandra Snyder for her excellent technical assistance and Dr. Jose Tomsig for help with the native gel electrophoresis. We are indebted to Dr. John Shannon for the N-terminal sequencing of annexin VI and Prof. Robert Huber for providing the structure coordinates of human wild-type annexin VI. Dr. Christine Wright is gratefully acknowledged for her advice in the crystallographic calculations of the T356D structure and Dr. Fraydoon Rastinejad for generously making available his X-ray equipment.

REFERENCES

1. Gerke, V., and Moss, S. E. (1997) Annexins and membrane dynamics, *Biochim. Biophys. Acta 1357*, 129−154.
2. Creutz, C. E. (1992) The annexins and exocytosis, *Science 258*, 924−951.
3. Rothhut, B. (1997) Participation of annexins in protein phosphorylation, *Cell. Mol. Life Sci. 53*, 522−526.
4. Smith, P. D., and Moss, S. E. (1994) Structural evolution of the annexin supergene family, *Trends Genet. 10*, 241−246.
5. Benz, J., Bergner, A., Hofmann, A., Demange, P., Gottig, P., Liemann, S., Huber, R., and Voges, D. (1996) The structure of recombinant human annexin VI in crystals and membrane-bound, *J. Mol. Biol. 260*, 638−643.
6. Avila-Sakar, A. J., Creutz, C. E., and Kretsinger, R. H. (1998) Crystal structure of bovine annexin VI in a calcium-bound state, *Biochim. Biophys. Acta 1387*, 103−116.
7. Avila-Sakar, A. J., Kretsinger, R. H., and Creutz, C. E. (2000) Membrane-bound 3D structures reveal the intrinsic flexibility of annexin VI, *J. Struct. Biol. 130*, 54−62.
8. Moss, S. E., Jacob, S. M., Davies, A. A., and Crumpton, M. J. A. (1992) Growth-dependent post-translational modification of annexin VI, *Biochim. Biophys. Acta 160*, 120−126.
9. Creutz, C. E., Kambouris, N. G., Snyder, S. L., Hamman, H. C., Nelson, M. R., Liu, W., and Rock, P. (1992) Effects of the expression of mammalian annexins in yeast secretory mutants, *J. Cell Sci. 103*, 1177−1192.
10. Wang, W., and Creutz, C. E. (1992) Regulation of the chromaffin granule aggregating activity of annexin I by phosphorylation, *Biochemistry 31*, 9934−9939.
11. Bradford, M. M. (1976) A rapid and sensitive method for the quantitation of microgram quantities of protein utilizing the principle of protein-dye binding, *Anal. Biochem. 72*, 248−254.
12. Pace, C. N. (1986) Determination and analysis of urea and guanidinium hydrochloride denaturation curves, *Methods Enzymol. 131*, 266−280.
13. Rodbard, D., and Chrambach, A. (1971) Estimation of molecular radius, free mobility, and valence using polyacylamide gel electrophoresis, *Anal. Biochem. 40*, 95−134.
14. Otwinowski, Z., and Minor, W. (1997) Processing of X-ray diffraction data collected in oscillation mode, *Methods Enzymol. 276*, 307−326.
15. Brünger, A. T., Adams, P. D., Clore, G. M., Deland, W. I., Gros, P., Grosse-Kunstleve, R. W., Jiang, J. S., Kuszewski, J., Nilges, M., Pannu, N. S., Read, R. J., Rice, L. M., Simonson, T., and Warren, G. I. (1998) Crystallography and NMR System: a new software suite for macromolecular structure determination, *Acta Crystallogr. D54*, 905−921.
16. Jones, T. A., and Kjeldgaard, M. (1992) *O, the Manual*, Pharmacia Biochem, Uppsala, Sweden.
17. Kaetzel, M. A., Mo, Y. D., Mealy, T. R., Campos, B., Bergsma-Schutter, W., Brisson, A., Dedman, J. R., and Seaton, B. A. (2001) Phosphorylation mutants elucidate the mechanism of annexin IV-mediated membrane aggregation, *Biochemistry 40*, 4192−4199.
18. Concha, N. O., Head, J. F., Kaetzel, M. A., Dedman, J. R., and Seaton, B. A. (1993) Rat annexin V crystal structure: Ca^{2+}-induced conformational changes, *Science 261*, 1321−1324.
19. Favier-Perron, B., Lewit-Bentley, A., and Russo-Marie, F. (1996) The high-resolution crystal structure of human annexin III shows subtle differences with annexin V, *Biochemistry 35*, 1740−1744.
20. Liemann, S., and Huber, R. (1997) Three-dimensional structure of annexins, *Cell. Mol. Life Sci. 53*, 516−521.
21. Meers, P., and Mealy, T. (1993) Relationship between annexin V tryptophan exposure, calcium, and phospholipid binding, *Biochemistry 32*, 5411−5418.
22. Bandorowicz-Pikula, J., and Pikula, S. (1998) Modulation of annexin VI-driven aggregation of phosphatidylserine liposomes by ATP, *Biochimie 80*, 613−620.
23. Blackwood, R. A., and Ernst, J. D. (1990) Characterization of Ca^{2+}-dependent phospholipid binding, vesicle aggregation and membrane fusion by annexins, *Biochem. J. 266*, 195−200.
24. Donnelly, S. R., and Moss, S. E. (1997) Annexins in the secretory pathway, *Cell. Mol. Life Sci. 53*, 533−538.

25. Wang, W., and Creutz, C. E. (1994) Role of the amino-terminal domain in regulating interactions of annexin I with membranes: effects of amino-terminal truncation and mutagenesis of the phosphorylation sites, *Biochemistry 33*, 275−282.
26. Fauvel, J., Vicendo, P., Roques, V., Ragab-Thomas, J., Granier, C., Vilgrain, I., Chambaz, E., Rochat, H., Chap, H., and Douste-Blazy, L. (1987) Isolation of two 67 kDa calcium-binding proteins from pig lung differing in affinity for phospholipids and in anti-phospholipase A2 activity, *FEBS Lett. 221*, 397−402.
27. Summers, T. A., and Creutz, C. E. (1985) Phosphorylation of a chromaffin granule-binding protein by protein kinase C, *J. Biol. Chem. 260*, 2437−2443.
28. Kenton, P., Johnson, P. M., and Webb, P. D. (1989) The phosphorylation of p68, a calcium-binding protein associated with the human syncitiotrophoblast submembranous cytoskeleton, is modulated by growth factors, activators of protein kinase C and cyclic AMP, *Biochim. Biophys. Acta 1014*, 271−281.
29. Stoehr, S. J., Smolen, J. E., and Suchard, S. J. (1990) Lipocortins are major substrates for protein kinase C in extracts of human neutrophils, *J. Immunol. 144*, 3936−3945.
30. Mani, R. S., and Kay, C. M. (1989) Purification and spectral studies on the Ca^{2+}-binding properties of 67 kDa calcimedin, *Biochem. J. 259*, 799−804.
31. Moore, P. B., and Dedman, J. R. (1984) Calmodulin, a calmodulin acceptor protein, and calcimedins: unique antibody localizations in hamster sperm, *J. Cell. Biochem. 25*, 99−107.
32. Porte, F., de Santa Barbara, P., Phalipou, S., Liautard, J. P., and Widada, J. S. (1996) Change in the N-terminal domain conformation of annexin I that correlates with liposome aggregation is impaired by Ser-27 to Glu mutation that mimics phosphorylation, *Biochim. Biophys. Acta 1293*, 177−184.
33. Myers, J. K., Pace, C. N., and Scholtz, J. M. (1995) Denaturant *m* values and heat capacity changes: relation of changes in accessible surface areas of protein unfolding, *Protein Sci. 4*, 2138−2148.
34. Guex, N., and Peitsch, M. C. (1997) SWISS-MODEL and the Swiss-PdbViewer: An environment for comparative protein modeling, *Electrophoresis 18*, 2714−2723.

BI026742H